Evolution of hardness, microstructure, and strain rate sensitivity in a Zn-22% Al eutectoid alloy processed by high-pressure torsion

2014 IOP Conf. Ser.: Mater. Sci. Eng. 63 012101

(http://iopscience.iop.org/1757-899X/63/1/012101)

IOP Conf. Series: Materials Science and Engineering **63** (2014) 012101 doi:10.1088/1757-899X/63/1/012101

Evolution of hardness, microstructure, and strain rate sensitivity in a Zn-22% Al eutectoid alloy processed by high-pressure torsion

Megumi Kawasaki [1,2,a], Han-Joo Lee [1,b], In-Chul Choi [1,c], Jae-il Jang [1,d], Byungmin Ahn [3,e] and Terence G Langdon [2,4,f]

[1] Division of Materials Science and Engineering, Hanyang University, Seoul 133-791, South Korea
[2] Departments of Aerospace & Mechanical Engineering and Materials Science, University of Southern California, Los Angeles, CA 90089-1453, U.S.A.
[3] Department of Energy Systems Research, Ajou University, Suwon, 443-749, South Korea
[4] Materials Research Group, Faculty of Engineering and the Environment, University of Southampton, Southampton SO17 1BJ, U.K.

E-mail: [a] megumi@hanyang.ac.kr, [b] hanjoolee@hanyang.ac.kr, [c] icchoi85@hanyang.ac.kr, [d] jijang@hanyang.ac.kr, [e] byungmin@ajou.ac.kr, [f] langdon@usc.edu

Abstract. Severe plastic deformation (SPD) is an attractive processing method for refining microstructures of metallic materials to give ultrafine grain sizes within the submicrometer to even the nanometer levels. Experiments were conducted to discuss the evolution of hardness, microstructure and strain rate sensitivity, *m*, in a Zn-22% Al eutectoid alloy processed by high-pressure torsion (HPT). The data from microhardness and nanoindentation hardness measurements revealed that there is a significant weakening in the Zn-Al alloy during HPT despite extensive grain refinement. Excellent room-temperature (RT) plasticity was observed in the alloy after HPT from nanoindentation creep in terms of an increased value of *m*. The microstructural changes with increasing numbers of HPT turns show a strong correlation with the change in the *m* value. Moerover, the excellent RT plasticity in the alloy is discussed in terms of the enhanced level of grain boundary sliding and the evolution of microsturucture.

1. Introduction

The application of processing through severe plastic deformation (SPD) provides a potential for fabricating ultrafine-grained (UFG) materials and bulk nanostructured materials with grain sizes in the submicrometer and even the nanometer ranges [1]. Among the SPD techniques, high-pressure torsion (HPT) is especially effective for producing UFG microstructures where a thin metal disk is subjected to an applied pressure and concurrent torsional straining [2]. In the HPT processing, the equivalent von Mises strain imposed by torsion straining on the disk, ε_{eq}, is given by the relationship [3-5]:

$$\varepsilon_{eq} = \frac{2\pi Nr}{h\sqrt{3}} \quad (1)$$

where r and h are the radius and height (or thickness) of the disk, respectively, and N is the number of HPT turns. It is apparent from eq (1) that the imposed strain is a maximum at the periphery of the disk but reduced with increasing distance from the center so that it becomes zero at the center of the disk. Thus, it is reasonable that both the microstructure and hardness are demonstrated with gradations with r across the disk in the early stages of HPT. However, since there is additional strain by compressive pressure during processing, sufficiently high numbers of HPT turns lead to reasonably homogeneous microstructures and local hardness throughout the disk [6,7].

There have been numerous trials of grain refinement for improving the superplastic properties in a Zn-22% Al alloy through conventional thermomechanical processing [8-16] and thermomechanical controlling process (TMCP) where conventional thermomechanical processing is conducted with several steps of well-controlled heat treatment [17-22], cross-channel extrusion [23], equal-channel angular pressing (ECAP) [24-37], friction stir processing (FSP) [38] and high-pressure torsion (HPT) [39-41]. These processing techniques led to refined grains of Zn-Al alloys to the submicrometer range so that the alloys exhibited excellent superplastic-like elongations of over 200% at room temperature (RT) [10,16-22,27,28,30,33,38]. Moreover, recent reports examined the capability of the RT superplastic properties and the low-work hardening rate in Zn-22% Al alloy for an application of tuned mass dampers to reduce seismic vibrations in building structures [18,20,22].

Nevertheless, there was no attempt to investigate the correlation between the changes in the UFG microstructure, the evolution in hardness and the RT plasticity in the Zn-22% Al alloy. Accordingly, this study was initiated to evaluate the evolution in hardness and in the values of strain rate sensitivity, m, calculated through nanoindentation testing of the Zn-Al alloy processed by HPT. The results are discussed in terms of the microstructural changes in the material through different numbers of HPT turns.

2. Experimental procedures

The experiments were conducted using a commercial Zn-22% Al eutectoid alloy containing the following impurities in ppm: Cr <10, Cu 20, Fe 70, Mg <10, Mn <10 and Si 70. The as-received alloy consisted of a binary microstructure with an Al-rich α phase and a Zn-rich β phase. The alloy was supplied in the form of a plate having a thickness of 25 mm and it was machined into a rod with a diameter of 10 mm and then cut into separate billets having lengths of ~60 mm. The rod was then sliced into disks having thicknesses of ~1.5-2.0 mm and each side of every disk was carefully polished using a Gatan Disk Grinder and abrasive papers to give a series of HPT disk samples having total parallel thicknesses of ~0.80 mm. The disks were annealed in air at 473 K for 1 h to remove any residual stresses before processing. This treatment gives a homogeneously distributed Al-phase in the Zn-rich matrix phase within the microstructure as shown in earlier reports [39,40]. It should be noted that the microstructure contains both of essentially equiaxed grains and of a lamellar structure. The average grain size in the equiaxed regions was measured as ~1.4 μm and the average thickness of ~100 nm was measured at thin layers of alternating α and β phases in the lamellar structure.

The processing by HPT was conducted using a quasi-constrained HPT [42,43] facility consisting of upper and lower anvils having circular depressions at the centers of the outer surfaces of each anvil with depths of 0.25 mm and diameters of 10 mm. Following the detailed procedure described earlier but without applying any lubricant around the anvil depths [44], a disk sample having a diameter of 10 mm and a thickness of ~0.80 mm was placed in the depression on the lower anvil and the anvil was moved upwards to a final position so that the disk was contained within the depressions on the two anvil surfaces under high compressive stress. In this study, a series of samples was processed under a fixed compressive pressure, P, of 6.0 GPa. Under compression, torsional straining was then applied to the disk by rotating the lower anvil in the same direction for total numbers of torsional revolutions, N, of 1, 2 or 4 turns at a fixed speed of 1 rpm.

The series of disks were mounted and polished carefully to obtain mirror-like surfaces and the values of the Vickers microhardness, Hv, were measured on the disk surfaces using an FM-1e microhardness tester equipped with a Vickers indenter. All hardness measurements were undertaken

with an indentation load of 100 gf and a dwelling time for each separate measurement of 15 s. As is apparent from eq (1), the variation in hardness is anticipated to appear in a radial direction and thus the hardness measurements were conducted along the diameter of each disk. In order to acquire a higher accuracy in the hardness values, the average values of *Hv* were determined at selected positions separated by incremental distances of 0.3 mm along a diameter in each disk. The average value of *Hv* at each selected position was determined from four separate measurements recorded at points uniformly arrayed by distances of 0.15 mm around the selected position.

Mechanical properties were examined at the edge of each disk using a nanoindentation facility, Nanoindenter-XP (formerly MTS; now Agilent, Oak Ridge, TN) with a three-sided pyramidal Berkovich indenter having a centerline-to-face angle of 65.3°. All measurements by nanoindentation testing were conducted at room temperature under a predetermined peak applied load of P_{max} = 20 mN at various indentation rates, $\dot{\varepsilon}_i$ [= $h_i^{-1}(\mathrm{d}h_i/\mathrm{d}t)$ where h_i is the indentation displacement and t is the loading time], of 0.0125, 0.025, 0.05 and 0.1 s^{-1}. To provide statistically valid data, more than 50 indentations were conducted under each measurement condition. Thermal drift was maintained below 0.1 nm/s in all experiments and the topological features of the indented surfaces were observed with a field-emission scanning electron microscope (FE SEM).

3. Results

3.1 Evolution of hardness across the disks after HPT

A series of disks was processed by HPT for 1, 2 and 4 turns at room temperature and the values of *Hv* were measured across the diameters of the disks. The results are summarized in a plot of *Hv* versus distance from the center as shown in Fig. 1 where, for comparison purposes, the hardness value of *Hv* ≈ 68 is indicated for the material after annealing without HPT processing [39,40]. The error bars in Fig. 1 correspond to the 95% confidence limits based on the separate measurements recorded around each point.

Figure 1 reveals several important characteristics of hardness evolution in the Zn-22% Al alloy after HPT with increasing numbers of turns. First, it is apparent that all the measured *Hv* values after HPT are lower than in the annealed condition without processing, thus demonstrating the occurrence of strain weakening in the alloy. This trend is different from the general hardness evolution associated with strain hardening observed in many commercial purity metals and alloys after HPT processing. A recent report summarizes the different models of hardness evolution in various metallic materials processed by HPT [45].

Second, there is a consistency in all of the disks that there is the occurrence of high *Hv* values in the centers of the disks and decreasing values towards the peripheries. Close inspection shows that the higher *Hv* values in the centers are typically larger by a factor of ~2 by comparison with the hardness values at the edges. Third, there is a decrease in the hardness values over the disk surfaces when processing is continued to larger numbers of turns. Practically, the *Hv* values decrease from ~60 to ~43 at the centers and from ~30 to ~23 at the peripheries through 1 to 4 turns, respectively. It should be noted that the difference in local hardness between the centers and peripheries in each disk tends to decrease thereby suggesting there is a gradual evolution towards hardness homogeneity in the Zn-Al alloy. Recent experiments showed detailed microstructural evolution through HPT in the Zn-Al alloy and only an equiaxed grain structure was observed at the peripheries of the processed disks whereas the centers of the disks contained dual structures with both equiaxed grains and a lamellar structure [39,40].

3.2 Mechanical testing by nanoindentation testing

Microhardness testing was conducted to the set of samples including the disk after annealing without processing (N = 0) and the results are shown in Figure 2 [46]. Figure 2a demonstrates representative load-displacement curves measured at an indentation strain rate of 0.025 s^{-1} for the samples of N = 0 to 4 and the load-displacement curves received at four different indentation rates are plotted for the sample of N = 0 and 4 in Figure 2b.

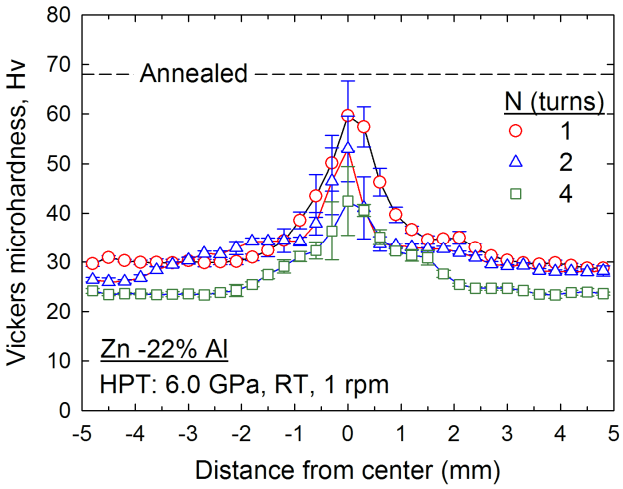

Figure 1. Variation of the average Vickers microhardness, *Hv*, with distance from the center of the Zn-22% Al disks processed by HPT for 1, 2 and 4 turns; the error bars denote the 95% confidence limits and the upper dashed line denotes the average hardness of the annealed material without processing. [39,40]

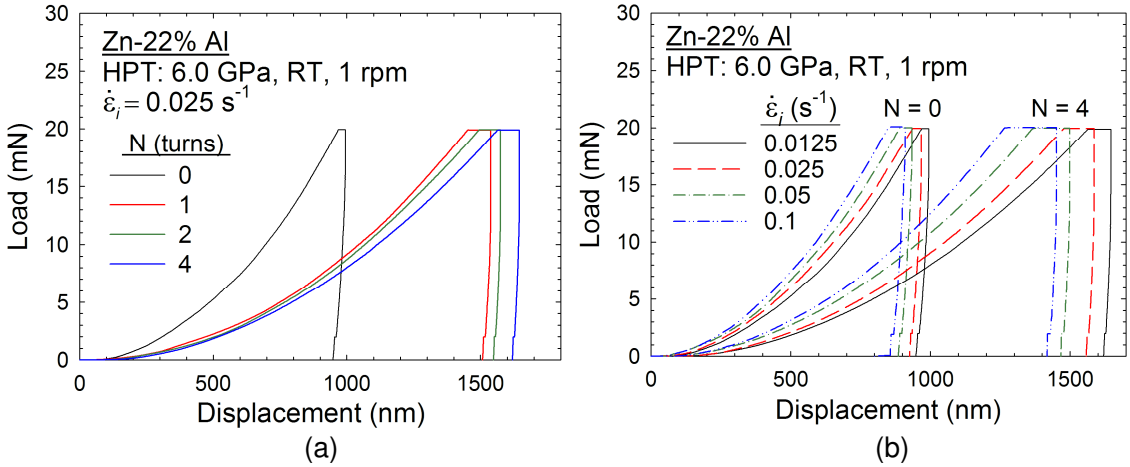

Figure 2. (a) Representative load-displacement curves measured at an indentation strain rate of 0.025 s^{-1} for the disks of N = 0 to 4 and (b) the curves taken at four different indentation rates for the samples of N = 0 and 4. [46]

It is apparent from Figure 2a that the samples processed by HPT deformed significantly compared with the sample without processing, thereby suggesting an excellent improvement upon RT plasticity in the Zn-Al alloy after HPT. In addition, the displacement increases with increasing numbers of HPT turns leading to a higher RT ductility with increasing numbers of N through 4 turns in the alloy. An inspection in Figure 2b shows the alloy both in an annealed condition without processing and after HPT demonstrates a consistent strain rate dependency on the peak load displacement.

From the data set of nanoindentation testing, the nanoindentation hardness, H, was estimated according to the Oliver-Pharr method [47] and Figure 3 shows the variation of H for the sample without processing and the samples after HPT with increasing numbers of HPT turns for the samples tested at 4 different indentation rates [46]. The Vickers microhardness values shown in Fig. 1 [39,40] were recalculated using the projected area instead of surface area so that a direct comparison is available between the H values estimated by nanoindentation testing and the hardness values calculated by the Vickers microhardness measurements.

It is apparent that, although there is a consist trend in the change of H for both measurements, the H values estimated through nanoindentation testing are higher than the recalculated values from Hv. This difference is explained by the indentation size effect where hardness increases as the indentation size decreases.

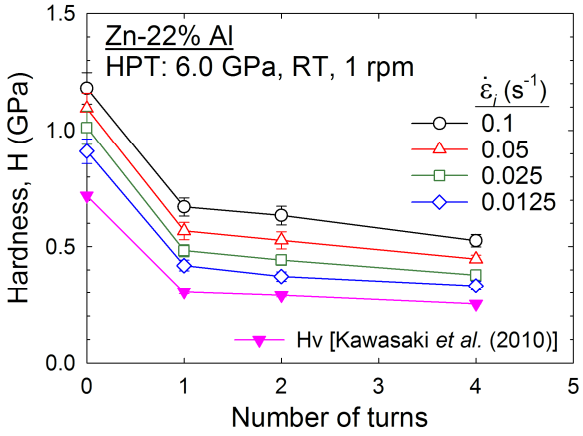

Figure 3. Variation of hardness with increasing numbers of HPT turns. The recalculated hardness shown in Figure 1 [39,40] is included for comparison purposes. [46]

From the nanoindentation hardness, it is seen at all indentation strain rates that the samples after HPT show significantly lower values of *H* compared with the sample without processing. In practice, the hardness decreases constantly with increasing numbers of turns. This is consistent with the results of *Hv* in Figure 1 and the nanoindentation testing also demonstrates a unique hardness evolution of strain weakening in the Zn-Al alloy after HPT.

3.3 Microstructure and the morphology of impressions in the Zn-Al alloy after HPT

Figure 4 shows SEM photos of the nanoindentation impressions at the edges of the disk in conditions (a) without HPT (N = 0) and after HPT for (b) 1, (c) 2 and (d) 4 turns after indentation under a constant load of 20 mN at an indentation rate of 0.025 s^{-1}, respectively [46]. The grains appearing white represent the major Zn-rich phase and the grains appearing black represent the Al-rich phase.

The background microstructure in the SEM photos provides important information of microstructural changes after HPT. The microstructure before processing included both equiaxed grains and a lamellar structure as shown in Figure 4a, but after HPT the microstructure at the edges of the disks no longer included a lamellar structure and there was a homogeneous microstructure consisting only of equiaxed fine grains as seen in Figures 4b-d. Moreover, there was an agglomeration of each phase in the early stage of HPT so that a banded structure of the UFG grains was formed after 1 and 2 turns as shown in Figures 4b-c whereas a fine microstructure with homogeneously distributed two phases appeared in the disk after 4 turns as shown in Figure 4d. There was significant grain refinement through HPT and close inspection showed that the average grain sizes were ~400 nm after 1 turn and ~350 nm after 2 and 4 turns. The ultrafine grain sizes in the Zn-22% Al alloy are consistent with the reported grain sizes of ~350 nm in a Zn-22% Al alloy processed by ECAP for 8 passes at RT [20,21] and ~380 nm in a Al-30% Zn alloy processed by HPT for 5 turns at RT [48,49].

The size of the nanoindentation impression was the smallest in the sample without HPT and it increases with increasing numbers of HPT turns. This confirms the decrease in both *H* and *Hv* with increasing numbers of HPT turns observed in Figures 1 and 3. The shear-off patterns around the indentation impressions are very clear in all samples whereas the behavior in the disk after 4 turns is less pronounced than in the other disks.

4. Discussion

In the present study, both Vickers microhardness and nanoindentation testing demonstrated the occurrence of strain weakening, rather than strengthening, in the Zn-Al alloy after HPT despite excellent grain refinement at the edges of the disks after processing. This phenomenon is reasonably explained by early TEM examinations showing a significant reduction in the distribution of rod-shaped precipitates of stable hexagonal close-packed Zn within the Al-rich grains which are visible in the annealed condition and the high pressure associated with SPD processing leads to an absorption of many of the Zn precipitates by the Zn-rich grains [50,51].

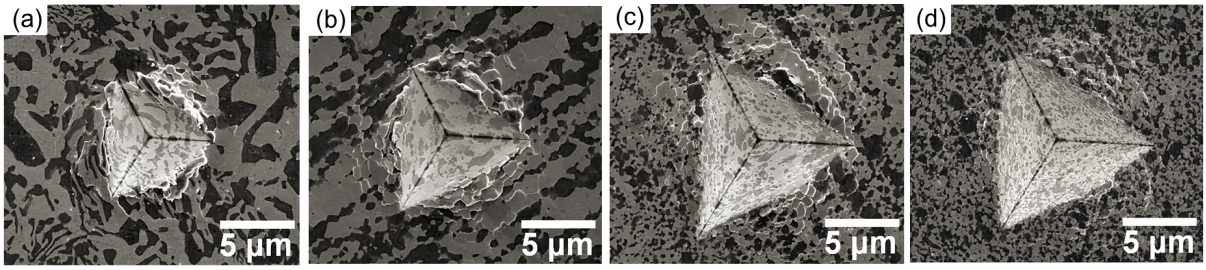

Figure 4. SEM photos of the nanoindentation impressions made under a constant maximum load of 20 mN at 0.025 s^{-1}on the edges of the disks for (a) $N = 0$, (b) $N = 1$, (c) $N = 2$ and (d) $N = 4$ [46].

It is worth noting that weakening phenomena was also observed in binary Al-10%-, 20%- and 30%-Zn alloys [45]. In the alloys, the Zn-rich supersaturated Al solid solution was decomposed during HPT and the phase in an equilibrium state remained, thus leading to a loss of the solid solution hardening.

On the contrary, the nanoindentation testing revealed superior RT plasticity in the disks after HPT. In order to understand the deformation characteristics at RT in the Zn-Al alloy after HPT, it is reasonable to evaluate the essential materials properties of strain rate sensitivity, m, from the data set of nanoindentation testing shown in Figures 2 and 3.

Considering Tabor's empirical prediction where the flow stress, σ_f, is equivalent to $H/3$ for fully plastic deformation at a constant strain rate, $\dot{\varepsilon}$ [53], the value of m is determined by the expression [54]:

$$m = \left(\frac{\partial \ln \sigma_f}{\partial \ln \dot{\varepsilon}} \right)_{\varepsilon,T} = \left(\frac{\partial \ln (H/3)}{\partial \ln \dot{\varepsilon}} \right)_{\varepsilon,T} \quad . \tag{2}$$

Applying the empirical relation of $\dot{\varepsilon} \approx \dot{\varepsilon}_i \times 10^{-2}\ s^{-1}$ [55,56], the value of m was calculated from the slope of the line for each sample in a logarithmic plot of $H/3$ versus $\dot{\varepsilon}$ as shown in Figure 5. It is apparent that the estimated m value for the sample without processing was enhanced significantly after HPT for 1 turn and it confirms the trend of enhanced plasticity by HPT as shown in Figure 2. There is an additional increase to reach a maximum value of $m \approx 0.265$ through two turns whereas the value decreases slightly after 4 turns. The m value for the sample without processing is reasonably within the range of the reported values of $m \approx 0.15$ for pure Zn [57] and ~0.02 for pure Al [58] and the high values of m after processing are in excellent agreement with the earlier reports showing the m values of ~0.25 to ~0.30 for a Zn-22% Al alloy after ECAP through 4 passes [27,28] and 8 passes [28] and tested at ~10^{-4} – 10^{-2} s^{-1}, respectively.

From the early literature, it is defined that superplastic ductility refers to exceptionally high elongations of >400% without necking when testing in tension at elevated temperatures of $T \geq 0.5T_m$ (T_m: the absolute melting temperature) [59]. In conventional superplastic metals including Zn-22% Al alloy, it is well known that the flow within the superplastic regime occurs by grain boundary sliding (GBS) [60]. Accordingly, because of the low T_m of the Zn-Al eutectoid alloy where RT corresponds to ~$0.44T_m$, the alloy exhibits excellent elongations at RT by the dominant deformation mechanism of GBS. The plastic deformation at RT controlled by GBS was observed earlier in the Zn-Al alloys processed through TMCP and measured by SEM [17] and processed by ECAP and measured by an atomic force microscope (AFM) [25,26].

The present nanoindentation testing demonstrated the improvement of plasticity in the Zn-Al alloy after grain refinement through HPT whereas there was a significant loss in hardness. Nevertheless, in the present examinations, there is a further change in the value of m with increasing numbers of HPT turns, thus implying a change in the nature of deformation in the Zn-Al alloy processed by HPT after different numbers of turns. This is explained by the correlation between the difference in the microstructure after HPT with increasing numbers of turns and the preferred interfaces for GBS in the Zn-Al alloy.

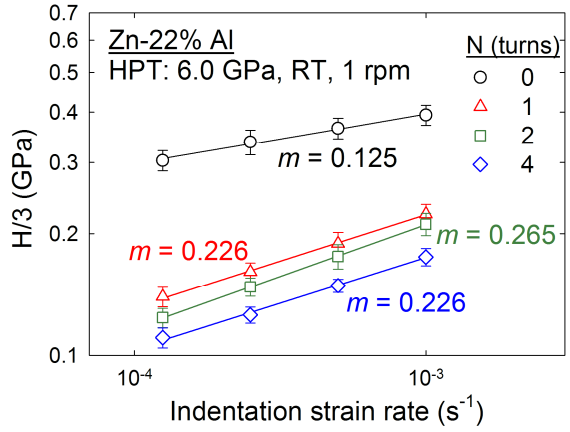

Figure 5. Variation of the values of *m* for the Zn-Al alloy before and after HPT for different numbers of turns. The *m* values were estimated as the slope of the line in the logarithmic plot of estimated flow stress versus indentation strain rates. [46]

Early GBS measurements by TEM showed that during the high temperature deformation there was a maximum contribution of GBS to the plastic deformation on the Zn-Zn interfaces and slightly less on the Zn-Al interfaces whereas the Al-Al interfaces exhibited a minimum contribution of GBS in the Zn-22% Al alloy without processing [61] and after ECAP [32,35,37]. Accordingly, as shown in Figures 4b-d, processing by HPT provided changes in the microstructure of the Zn-Al alloy where the grain sizes were further reduced from 1 to 2 turns and the banded structure of Zn- and Al- rich phases disappeared after 4 turns. Therefore, the samples after HPT for 1 and 2 turns contain large numbers of Zn-Zn interfaces which are preferred for demonstrating a high level of GBS while there is an increased and decreased numbers of Zn-Al and Zn-Zn interfaces, respectively, after 4 turns. Thus, with pronounced grain refinement, the level of GBS was improved with increasing numbers of revolutions through 2 turns, thereby showing the highest value of *m*, but subsequently declined slightly thorough 4 turns due to the homogeneous distributions of the two phases.

Nevertheless, the values of *m* observed in the present experiments are very high for RT plasticity because of the enhanced level of GBS by grain refinement through HPT leading to the introduction of a great number of grain boundaries in the samples. There are several experiments reporting *m* values of over 0.2 during deformation at RT in various Zn-Al (and Al-Zn) alloys prepared by different processing techniques including ECAP and HPT and it is worth summarizing the data with the values of *m* in Table A1 in the Appendix.

Finally, there is a very resent investigation on an Al-30% Zn alloy by nanoindentation and compression testing using nano-pillers showing that, although a similar type of weakening is found in nano-hardness after HPT, there is an improved RT plastic behavior compared with the coarse-grained Al-Zn alloy [62]. For the alloy, the improved plasticity was acquired by enhancing the rule of GBS at the Al-Al interfaces by the formation of a Zn-rich layer through HPT processing. Thus, it is anticipated that the SPD techniques including ECAP and HPT provide a great potential of achieving advancing mechanical properties in UFG metals using grain boundary engineering.

5. Summary and conclusions

This study through nanoindentation testing demonstrates a unique hardness evolution of weakening and improved RT plasticity with high values of *m* in the Zn-22% Al alloy processed by HPT. The change in the values of *m* with increasing numbers of HPT turns is explained by the level of GBS attributed to the microstructural evolution involving the formation of preferred interfaces.

Acknowledgements

This research was supported by the National Research Foundation of Korea (NRF) grant funded by the Korea government (MSIP) (No. 2013R1A1A2A100 58551). The work at USC and the University of Southampton was supported in part by the National Science Foundation of the United States under Grant No. DMR-1160966 and in part by the European Research Council under ERC Grant Agreement No. 267464-SPDMETALS.

Appendix

Table A1. A list of Zn-Al alloys processed through different processing techniques showing the high values of strain rate sensitivity, *m*, at specific strain rate ranges at room temperature measured using different testing methods.

Materials (wt.%)	Processing	Grain size (μm)	Testing method	*m*	Strain rate range (s^{-1})	References
Al-30Zn	HPT for 5 turns at RT	~0.38	Tensile testing	~0.29	10^{-4}- 10^{-3}	Valiev *et al.* (2010) [48]
Al-30Zn	HPT for 5 turns at RT	~0.38	Microindentaion	~0.22	6.25×10^{-5} - 1.75×10^{-2}	Chinh *et al.* (2012) [49]
Zn-0.3Al	Cold rolling	1	Tensile testing until strain of 10%	0.41	10^{-4}- 10^{-3}	Ha *et al.* (1997) [63], Ha *et al.* (2001) [64]
Zn-0.3Al	Cold rolling	1	Tensile testing until strain of 2.5%	0.32	10^{-6}- 10^{-4}	Ha *et al.* (2001) [64]
Zn-0.4Al	Cold rolling	~0.6	Tensile testing	0.4-0.5	10^{-4}- 10^{-3}	Naziri and Pearce (1974) [65]
Zn-2Al Zn-10Al Zn-22Al Zn-50Al	Casting + quenching + annealing at 523 K	~1	Tensile testing	0.40 0.43 0.45 0.43	10^{-3}- 10^{-2}	Kaibyshev *et al.* (1978) [10]
Zn-20Al	Hot rolling + quenching	0.55	Tensile deformation at *in-situ* TEM	0.25	10^{-3}-10^{-1}	Naziri *et al.* (1975) [66]
Zn-22Al-2Cu	Cold rolling at 293 K	~0.3	Tensile testing	0.3	10^{-4}- 10^{-3}	Torres-Villaseñor and Negrete (1997) [16]
Zn-22Al	TMCP (Rolling)	1.3	Tensile testing	0.3	10^{-5}- 10^{-4}	Tanaka *et al.* (2002) [17]
Zn-22Al	TMCP (Extrusion)	~0.9	Tensile testing	0.3	10^{-5}- 10^{-2}	Tanaka *et al.* (2003) [18]
Zn-22Al	TMCP (Extrusion) + Cold rolling at RT	1.25	Tensile testing	0.25	10^{-5}- 10^{-2}	Tanaka and Higashi (2004) [19]
Zn-22Al	TMCP (Extrusion) TMCP (Rolling)	1.84 1.16	Tensile testing	~0.33	10^{-4}- 10^{-3} 10^{-4}- 10^{-2}	Tanaka and Higashi (2005) [21]
Zn-22Al	ECAP for 4p at RT	0.35	Tensile testing	0.25	10^{-4}- 10^{-2}	Tanaka and Higashi (2004) [27], Tanaka *et al.* (2004) [28]
Zn-22Al	ECAP for 8p at RT ECAP for 8p at 373 K	0.3 0.6	Tensile testing	~0.3	10^{-5}- 10^{-2}	Tanaka *et al.* (2004) [28]
Zn-22Al	Quenching + aging at RT ECAP for 8p at RT Cryo-rolling at 203 K	0.35 0.55 0.25	Tensile testing	0.38 0.35 0.32	10^{-2}- 10^{-1} 10^{-2}- 10^{-1} 10^{-3}- 10^{-2}	Xia *et al.* (2008) [33]
Zn-22Al	FSP	0.6	Tensile testing	0.25	10^{-4}- 10^{-2}	Hirata *et al.* (2007) [38]
Zn-22Al	HPT for ~4 turns at RT	0.35	Nanoindentation	0.265	10^{-4}- 10^{-3}	Choi *et al.* (2014) [46]

References

[1] Valiev RZ, Estrin Y, Horita Z, Langdon TG, Zehetbauer MJ and Zhu YT 2006 *JOM* **58** (4) 33
[2] Zhilyaev AP and Langdon TG 2008 *Prog. Mater. Sci.* **53** 893
[3] Valiev RZ, Ivanisenko YuV, Rauch EF and Baudelet B 1996 Acta Mater. **44** 4705
[4] Wetscher F, Vorhauer A, Stock R and Pippan R 2004 *Mater. Sci. Eng. A* **387-389** 809
[5] Wetscher F, Pippan R, Sturm S, Kauffmann F, Scheu C and Dehm G 2006 *Metall. Mater. Trans. A* **37A** 1963
[6] Xu C, Horita Z and Langdon TG 2008 *J. Mater. Sci.* **43** 7286
[7] Zhilyaev AP, Oh-ishi K, Langdon TG and McNelley TR 2005 *Mater. Sci. Eng. A* **410–411** 277
[8] Ishikawa H, Mohamed FA and Langdon TG 1975 *Phil. Mag.* **32** 1269
[9] Ishikawa H, Bhat DG, Mohamed FA and Langdon TG 1977 *Metall. Trans.* **8A** 523
[10] Kaibyshev OA, Rodionov BV and Valiev RZ 1978 *Acta Metall.* **26** 1877
[11] Miller DAand Langdon TG 1978 *Metall. Trans.* **9A** 1688
[12] Miller DA and Langdon TG 1979 *Metall. Trans.* **10A** 1869
[13] Ahmed MMI, Mohamed FA and Langdon TG 1979 *J. Mater. Sci.* **14** 2913
[14] Langdon TG 1982 *Metal. Sci.* **16** 175
[15] Chokshi AH and Langdon TG 1989 *Acta Metall.* **37** 715
[16] Torres-Villaseñor G and Negrete J 1997 *Mater. Sci. Forum* **243–245** 553
[17] Tanaka T, Makii K, Kushibe A and Higashi K 2002 *Mater. Trans.* **43** 2449
[18] Tanaka T, Makii K, Kushibe A, Kohzu M and Higashi K 2003 *Scripta Mater.* **49** 361
[19] Tanaka T and Higashi K 2004 *Mater. Trans.* **45** 2547
[20] Makii K, Furuta S, Aoki K, Kushibe A, Tanaka T and Higashi K 2004 *Mater. Sci. Forum* **447-448** 497
[21] Tanaka T, Kohzu M, Takigawa Y and Higashi K 2005 *Scripta Mater.* **52** 231.
[22] Kushibe A, Takigawa Y, Higashi K, Aoki K, Makii K and Takagi T 2007 *Mater. Sci. Forum* **551-552** 583
[23] Chou C-Y, Lee S-L, Lin J-C and Hsu C-M 2007 *Scripta Mater.* **57** 972
[24] Furukawa M, Ma Y, Horita Z, Nemoto M, Valiev RZ and Langdon TG 1998 *Mater. Sci. Eng. A* **241** 122
[25] Huang Y and Langdon TG 2002 *J. Mater. Sci.* **37** 4993
[26] Huang Y and Langdon TG 2003 *Mater. Sci. Eng. A* **358** 114
[27] Tanaka T and Higashi K 2004 *Mater. Trans.* **45** 1261
[28] Tanaka T, Watanabe H, Kohzu M and Higashi K 2004 *Mater. Sci. Forum* **447-448** 489
[29] Kumar P, Xu C and Langdon TG 2005 *Mater. Sci. Eng. A* **410–411** 447
[30] Kumar P, Xu C and Langdon TG 2006 *Mater. Sci. Eng. A* **429** 324
[31] Kawasaki M and Langdon TG 2008 *J. Mater. Sci.* **43** 7360
[32] Kawasaki M and Langdon TG 2008 *Mater. Trans.* **49** 84
[33] Xia SH, Wang J, Wang JT and Liu JQ 2008 *Mater. Sci. Eng. A* **493** 111
[34] Tanaka T, Kushibe A, Kohzu M, Takigawa Y and Higashi K 2009 *Scripta Mater.* **59** 215
[35] Kawasaki M and Langdon TG 2009 *Mater. Sci. Eng. A* **503** 48
[36] Kawasaki M and Langdon TG 2012 *Mater. Trans.* **53** 87
[37] Kawasaki M and Langdon TG 2013 *J. Mater. Sci.* **48** 4730
[38] Hirata T, Tanaka T, Chung SW, Takigawa Y and Higashi K 2007 *Scripta Mater.* **56** 477.
[39] Kawasaki M, Ahn B and Langdon TG 2010 *Acta Mater.* **58** 919
[40] Kawasaki M, Ahn B and Langdon TG 2010 *Mater. Sci. Eng. A* **527** 7008
[41] Kawasaki M and Langdon TG 2011 *Mater. Sci. Eng. A* **528** 6140
[42] Figueiredo RB, Cetlin PR and Langdon TG 2011 *Mater. Sci. Eng. A* **528** 8198
[43] Figueiredo RB, Pereira PHR, Aguilar MTP, Cetlin PR and Langdon TG 2012 *Acta Mater.* **60** 3190
[44] Kawasaki M and Langdon TG 2008 *Mater. Sci. Eng. A* **498** 341
[45] Kawasaki M 2014 *J. Mater. Sci.* **49** 18.

[46] Choi I-C, Kim Y-J, Ahn B, Kawasaki M, Langdon TG and Jang J-i 2014 *Scripta Mater.* **75** 102
[47] Oliver WC and Pharr GM 1992 *J. Mater. Res.* **7** 1564
[48] Valiev RZ, Murashkin MYu, Kilmametov A, Straumal B, Chinh NQ and Langdon TG 2010 *J. Mater. Sci.* **45** 4718
[49] Chinh NQ, Csanádi T, Győri T, Valiev RZ, Straumal BB, Kawasaki M and Langdon TG 2013 *Mater. Sci.Eng. A* **543** 117
[50] Furukawa M, Horita Z, Nemoto M, Valiev RZ and Langdon TG 1996 *J. Mater. Res.* **11** 2128
[51] Furukawa M, Ma Y, Horita Z, Nemoto M, Valiev RZ and Langdon TG 1998 *Mater. Sci. Eng. A* **241** 122.
[52] Mazilkin AA, Straumal BB, Rabkin E, Baretzky B, Enders S, Protasova SG, Kogtenkova OA and Valiev RZ 2006 *Acta Mater.* **54** 3933
[53] Shim S, Jang J-i and Pharr GM 2008 *Acta Mater.* **56** 3824
[54] Choi I-C, Kim Y-J, Wang YM, Ramamurty U and Jang J-i 2013 *Acta Mater.* **61** 7313
[55] Wang CL, Lai YH, Huang JC and Nieh TG 2010 *Scripta Mater.* **62** 175
[56] Choi I-C, Yoo B-G, Kim Y-J, Seok M-Y, Wang YM and Jang J-i 2011 *Scripta Mater.* **65** 300
[57] Zhang X, Wang H, Scattergood RO, Narayan J, Koch CC, Sergueeva AV and Mukherjee AK 2002 *Acta Mater.* **50** 4823
[58] Miyamoto H, Ota K and Mimaki T 2006 *Scripta Mater.* **54** 1913.
[59] Langdon TG 2009 *J. Mater. Sci.* **44** 5998
[60] Langdon TG 1994 *Mater. Sci. Eng. A* **174** 225
[61] Shariat P, Vastava RB and Langdon TG 1982 *Acta Metall.* **30** 285.
[62] Chinh NQ, Valiev RZ, Sauvage X, Varga G, Havancsák K, Kawasaki M, Straumal BB and Langdon TG 2014 *Adv. Eng. Mater.* **In-press**
[63] Ha TK, Lee WB, Park CG and Chang YW 1997 *Metall. Mater. Trans. A* **28A** 1771
[64] Ha TK, Son JR, Lee WB, Park CG and Chang YW 2001 *Mater. Sci. Eng. A* **307** 98
[65] Naziri H and Pearce R 1974 *Acta Metall.* **22** 1321.
[66] Naziri H, Pearce R, Brown MH and Hale KF 1975 *Acta Metall.* **23** 489